Iodide-Capped PbS Quantum Dots: Full Optical Characterization of a Versatile Absorber

Philipp Stadler, Shaimaa A. Mohamed, Jacek Gasiorowski, Mykhailo Sytnyk, Sergii Yakunin, Markus C. Scharber, Christina Enengl, Sandra Enengl, Daniel A. M. Egbe, Mabrouk K. El-Mansy, Salah S. A. Obayya, N. Serdar Sariciftci, Kurt Hingerl, and Wolfgang Heiss*

Colloidal semiconductor nanocrystal routes represent an attractive alternative compared to various vacuum-based techniques in order to obtain optoelectronic devices. It is the solution-processibility, which opens up new prospects in implementing thin-films on large areas. Photovoltaic cells, for example, have been successfully demonstrated using a colloidal approach—nanocrystallline CdTe or CuInSe cells exhibiting power conversion efficiencies ≥10% have been achieved recently.[1,2]

By virtue of the colloidal route bulk semiconductor properties can be tuned via the quantum size effect: Quantum dots (QD)—nanocrystals having dimensions below their semiconductor's exciton radii—liberate the material portfolio from the classic photovoltaic materials: The absorption-emission of low-gap semiconductors can be shifted from the deep infrared toward the visible range to match to the solar spectrum. Combined with an efficient luminescence quantum yield QDs represent a promising absorber material. Lead-sulfide (PbS) as an example holds the record within QD-approaches: Monodisperse, stable solutions have been size-shifted to a peak emission at 1.34 eV and implemented in thin-film solar cells achieving power-conversion efficiencies (PCEs) greater than 7%.[3–6]

Although these photovoltaic cells apply optimized designs, the full potential is not harnessed yet. It is the QD's thin-film properties, which still limit the performance—thus we sought for resolving the thin film's optical properties in greater detail and, based on that, develop strategies to overcome existing limits: To our opinion it is the treatment route—the development of the final QD thin solid film—which has to be understood to greater excess.

Here we point at the crucial difference between high performing solar cells from CdTe and CuInSe nanocrystals and that of PbS quantum dots. In the former case one pursues sintering, resulting in a bulk-like polycrystalline solid, whereas exactly this strategy has to be avoided in the case of PbS-QDs. Such a treatment would transform the system into a semiconductor with a bandgap energy deep in the mid-infrared—an unwanted scenario for photovoltaic applications. Contrariwise, in the case of QDs properties have to be carefully preserved. Quantum confined states are still required to end up with absorption edges suitable for solar harvesting, meaning that thin films of separate quantum dots are required. At the same time the quantum confined states have to be sufficiently coupled to allow an electrical transport through the film. This obvious contradiction is resolved with a compromise: By replacing the bulky surfactants from the colloidal phase with tiny functional molecules the interdot spacing is reduced and QDs couple with keeping their optical signatures.

Variable ligand strategies have been applied that emphasizes either optical properties or transport.[5,7–9] We took the view on one particular system, which represents a good compromise with respect to both. The approach applies iodide that replaces the oleate in colloidal PbS-nanocrystals.[7] Charge carrier mobilities and power conversion efficiency values reported are record-holding.[5,6,10,11] In this work we focus on an in-depth optical understanding while processing an iodide-treated QD thin solid film. Therefore, we deploy various spectroscopic tools, in order to elucidate the system from different point of views. Our study stresses the ambivalent nature of a QD thin solid film as intermediate between bulk and strictly confined states. We investigate the system's transition using spectroscopic ellipsometry including consistent optical parameters on a representative spectral range for all mentioned stages.[12,13] In parallel, we perform an absorption-emission tracking including also time resolved photoluminescence and vibrational aspects. Our insights help us to demonstrate a single-junction solar cell, which reaches a state-of-the-art performance without applying elaborate device architectures to optimize charge carrier harvesting.[5,6] The full optical response and our photovoltaic results allow us to evaluate the opportunities and limits of QD thin solid films—with an eye on understanding the material's

Dr. P. Stadler, S. A. Mohamed, M. C. Scharber, C. Enengl, S. Enengl, D. A. M. Egbe, N. S. Sariciftci
Linz Institute for Organic Solar Cells (LIOS)
Physical Chemistry
Johannes Kepler University Linz
Altenbergerstr. 69, A-4040 Linz, Austria
E-mail: philipp.stadler@jku.at

S. A. Mohamed, M. K. El-Mansy
Department of Physics
Benha University
Stadium Street 13518 Benha, Egypt

S. A. Mohamed, S. S. A. Obayya
Center for Photonic and Smart Materials (CPMS)
Zewail City of Science and Technology
Sheikh Zayed District, 6th of October City, 12588 Giza, Egypt

J. Gasiorowski, K. Hingerl
Center for Surface- and Nanoanalytics
Johannes Kepler University
Linz, Altenbergerstr. 69, A-4020 Linz, Austria

M. Sytnyk, S. Yakunin, W. Heiss
Institute of Semiconductor and Solid State Physics
Johannes Kepler University Linz
Altenbergerstr. 69, A-4040, Linz, Austria

DOI: 10.1002/adma.201404921

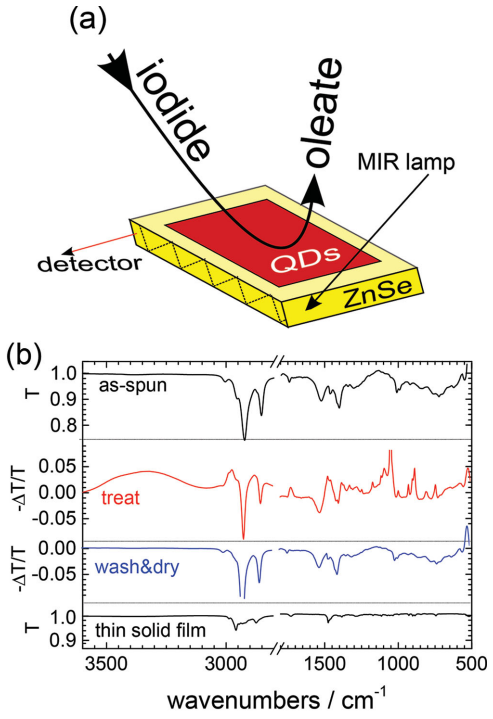

Figure 1. Vibronic response when processing QDs to the thin-film solid using ATR-FTIR. In (a) a sketch of the in situ ATR-setup (flow-cell with the ligand-substitution medium mounted on top of the ZnSe crystal). In (b) the transmission FTIR spectra of as-spun QDs and the final thin solid film are presented. In between we plot differential scans during exposure to medium (EtOH, TBA-I) and during the wash&dry process. The negative peaks correspond the oleate depletion during treatment, positive peaks to emergence of new signals such as the medium. The treated thin solid film exhibits weak IR-modes with respect to the initial scans indicating quantitative substitution of oleate by iodide.

potential and limits and on future concepts to tailor QDs for efficient optoelectronic device applications.

As mentioned above the importance of the nanocrystal processing route is outlined to be crucial for the performance of the final devices. Since recently iodine-processed PbS QD solids have been used to obtain record device efficiencies, in the following we elaborate in detail the changes of the optical properties during QD solid preparation, observed in particular for the iodide based ligand treatment process. These insights show the potentials and the limits in QD active layers for photovoltaic devices.[14,15] First, we take the view to the vibronic changes related to the substitution of bulky oleate chains with iodide. In **Figure 1** we pursue a careful spectral tracking by FTIR-ATR: Changes inside the QD processing are highlighted in transmission (T) and corresponding differential absorption ($-\Delta T/T$) spectra.

The spectrum of as-spun QDs correlates 1:1 to oleate (Figure 1)—we resolve the detailed vibrational terms in the Supporting Information. During treatment with iodide solution (treat) our in situ tracking shows positive solution peaks (ethanol) and negative oleate vibrations in the $\Delta T/T$-spectrum. Negative oleate peaks are seen after the consecutive wash&dry step as well—both steps lead to the intended quantitative oleate depletion. The final transmission plot of treated, solid QDs exhibits weak IR-modes—they relate to remaining traces of oleate. Due to the FTIR-ATR-mode (5-fold internal reflection with an amplified signal), we desist from any quantitative statements. Nevertheless we can clearly see that the preponderance of the bulky ligand has been replaced with iodide and the system has been transformed from initially diluted nanocrystals into a compact QD thin solid film.

The ligand exchange also affects excitonic- and interband absorption, as is shown in detail in **Figure 2**a. Interestingly, the

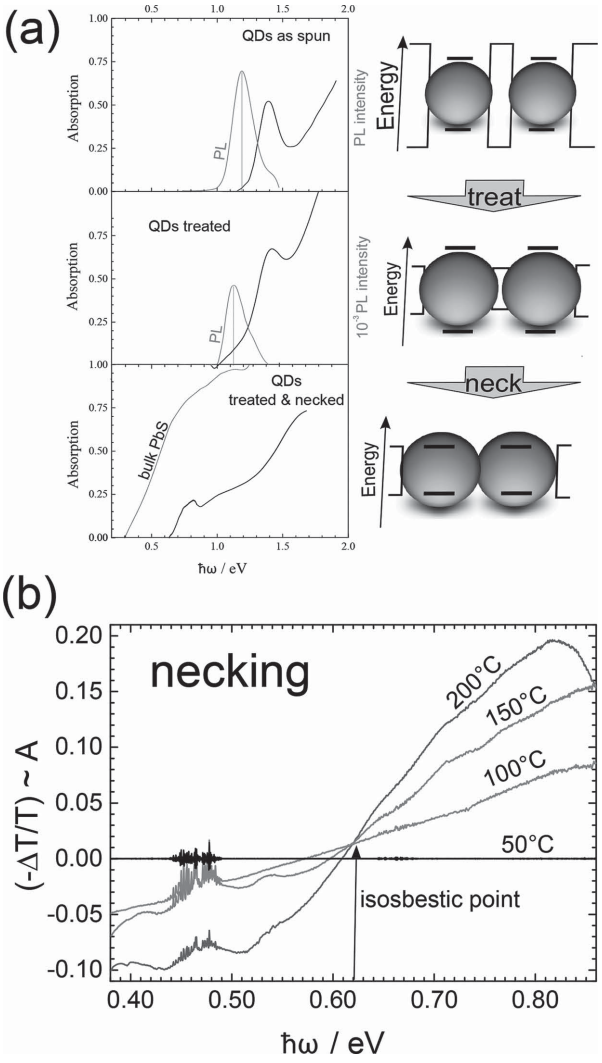

Figure 2. a) Plot of the absorption and emission spectra in the energy region of the exciton at 1.23 eV for all stages: As-spun, treated, and necked QDs. While as-spun and treated QDs exhibit their main absorption and emission feature according to the quantum size effect, thermal overtreatment say necking partly quenches these features—the necked QD's band edge moved toward the bulk phase in the mid-IR. b) The absorption response therein shows the effect of annealing of treated QDs (testing room temperature to 200 °C). Starting from 100 °C a positive signal arises at higher energies correlating to an absorption feature ($-\Delta T/T \approx$ absorbance). On the low energy side of the spectrum, the signals shift to the negative—an indication for a change of the dielectric function (and hence reflectivity). All scans coincide at the isosbestic point (0.62 eV) in the center—it confirms that a consistent chemical reaction is taking place, which gets more intense at higher temperatures. We interpret the isosbestic point as an absorption- or band edge due to necking—it is a strong argument for loosing the quantum confinement regime partly.

position of the excitonic absorption and emission peak before and after iodine treatment and drying at 50 °C practically coincide—indicating that QDs in the film remain in a confined state. Treatments above 50 °C, however, behave severely different: Here the absorption edge has been moved toward the bulk phase—at the same time we are no longer able to identify an excitonic absorption and emission feature.[16]

In order to study the mentioned absorption edge shift more precisely we apply the FTIR-ATR setup again (Figure 2b). Now we elucidate the electronic changes in the vicinity of bulk PbS's edge at 0.43 eV. For this we stepwise expose treated QDs to higher temperatures while recording spectra, which are then referenced to a room temperature control sequence. The final differential spectrum ($-\Delta T/T$) depicts changes in absorption induced by annealing: At 50 °C, for instance, the absorption remains unchanged seen in a flat line. Hence we conclude QDs are confined say intact. Differently, at 100 °C we observe significant deviations, which amplify further by increasing the temperature. Interestingly, these changes are systematic, as all spectra taken above 100 °C reflect the same trend and coincide at an isosbestic point (0.62 eV): Below that point the signals decrease to the negative, while above a positive rise is seen. The latter correlates to an absorption feature, while the negative signal mirrors changes in the material's dielectric function. It is the isosbestic point in particular that confirms a continuous and consistent chemical transition—from initially intact and transparent QDs to nanocrystals now having an interband absorption edge. We interpret the results as a quantitative merging, a sintering of QDs: Sometimes these processes are also described as necking—it is depicted as a direct attachment of nanocrystal facets. Annealing already has been investigated to trigger necked PbS- and related nanocrystals.[17–19] Our experiments now provide insight to the electronic changes undergone during necking: Exactly the mentioned bulk scenario is established, which we wanted to avoid in light-harvesting devices. After loosing their excitonic character, the QD's lowest energy transition is defined by the red-shifted absorption edge at 0.62 eV, which has been likewise induced by the iodide and organic residues at the nanocrystal surface.[20]

We conclude that—with respect to the intended goal photovoltaic applications—thermal overtreatment—drying at temperatures above 50 °C—has to be avoided. Furthermore, we concentrate on the ligand exchange itself that has rendered an intact QD system and display the differences herein. Though both systems—oleate- and iodide-QDs—exhibit the fingerprint excitonic features in Figure 2a, we do see distinct changes that have been induced by the ligand exchange: One is an altered absorption profile and a nominally increased absorbance. Another one affects the quenching of the PL.

To resolve the latter issue more clearly, we include a time-resolved PL study presented in **Figure 3**. We plot the normalized intensities $\phi(t)$ for oleate and iodide capped QDs: The time constant τ drops from 400 ns (as-spun) to 1.8 and 8.0 ns, respectively (treated). Similar values have been reported earlier for various QD treatment strategies.[21] While oleate-QDs follow an exponential decay, the quenching response of iodide-QDs

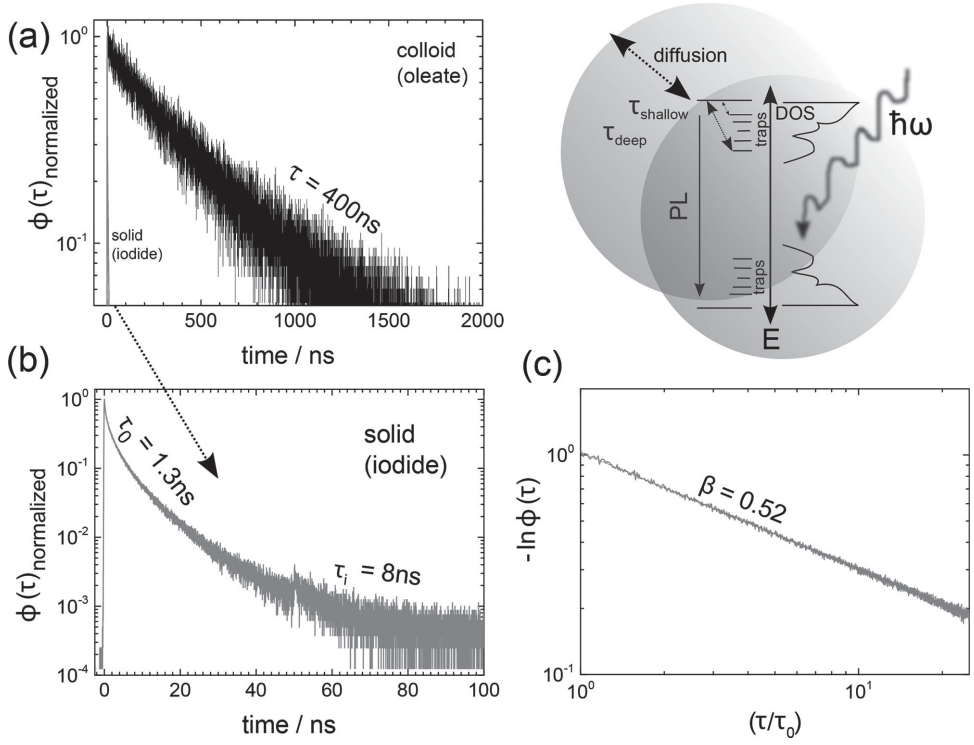

Figure 3. a) The time-resolved photoluminescence response $\varphi(\tau)$ reveals a different time regime before and after ligand exchange of QD thin films. The intensity decay in the solid in (b) shows the reduced carrier lifetimes and a solution for the underlying quenching process. The time constants split up to a series of τs (indicated by τ_0, τ_i) following a stretch-exponential model. Its linear fit and the exponent β is plotted in (d)—the latter is interpreted as a measure for a distribution of various recombination processes as illustrated in (c).

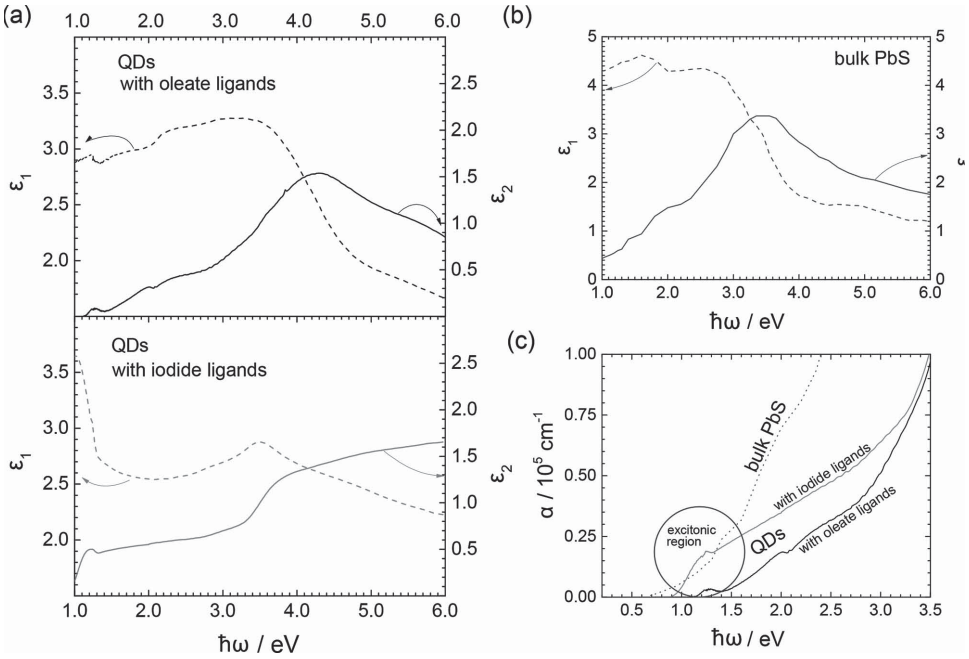

Figure 4. We present the dielectric functions of QDs with oleate ligands and QDs treated with iodide thereafter (a) and bulk PbS included as a reference (b), courtesy of Palik et al.[23]. For the oleate-capped QDs (as-spun from colloidal solution) a Bruggeman model is applied. Differently, the treated QDs with iodide ligands are fitted using a Cauchy model. The comparison of between oleate-capped QDs and iodide-capped QDs shows the deep impact of the ligand exchange on the dielectric function and hence all optical parameters. One example is seen in (c)—the spectrally resolved absorption coefficients α for all stages is modified between QDs having oleate-ligands and QDs with iodide-ligands. We add bulk PbS for direct comparison in (b) and (c).

split up into a series of time regimes—starting with the most dominant one τ_0 to finally τ_i. We apply a stretch-exponential model and plot a corresponding ln $\varphi(\tau)$ plot in Figure 3c including a linear fit: Epshtein et al[22] characterize the stretch exponent β as an indicator for disorder—it reflects a distribution of lifetimes with different quenching processes: shallow and deep traps as well as interdot diffusion. The formula for calculating β corresponds to:

$$\phi(\tau) = \exp[-(\tau/\tau_0)^{\beta}] \text{ with } 0 < \beta < 1 \quad (1)$$

with a value of 0.5 for β. The results reveal that lifetimes become shorter after ligand exchange. β indicates that the underlying quenching processes are complex and of diverse origin: surface-defects play a dominant role initially. The extended lifetime response thereafter indicates rather carrier diffusion in the film. It is in particular the atomic ligands approach that couples QDs efficiently achieving record charge carrier mobilities.[10,11] Thus diffusion and self-quenching within the film explain, why the material's performances in radiative devices is reasonable despite of the quenching's significance.

Similarly we also resolve the absorbance spectra in Figure 2a in greater detail: They are deduced from transmittance experiments by neglecting reflectance. This approach might provide misleading results, because also reflectance undergoes changes upon ligand exchange. Thus, we have chosen a more precise optical technique that rules out possible scattering and interference effects. Angle resolved spectroscopic ellipsometry (VASE) provides profound insights—in particular in materials exhibiting shifted energy states due to quantum-confinement it is crucial to determine the dielectric function based on an consistent optical model: In both the QDs having oleate- and iodide-passivation an effective medium approximation is reasonable, as for the spectroscopic region of interest the incident wavelength exceeds the nanocrystal's dimensions significantly ($\lambda_{incident} \gg d_{nanocrystal}$). We pick the data from volume PbS[23] and match its parameters to an optical quantum dot model accordingly. QDs with oleate ligands fit to the ideal case of nanocrystals-in-matrix (Bruggeman-model): Diluted bulk PbS shifted by quantization. Differently, QDs with iodide ligands are modeled as a homogenous semiconductor layer by a Cauchy approach assuming the iodide to be part of the QDs and voids. The corresponding real $\varepsilon_1(\omega)$ and imaginary $\varepsilon_2(\omega)$ and the absorption coefficients for all stages (QDs with oleate ligands, QDs with iodide ligands, bulk PbS) are summarized in **Figure 4**.

The dielectric response reveals similarities and differences before and after ligand exchange. The excitonic absorption at 1.23 eV as one example is conserved. The closer packing by tiny iodide leads to an increase in the absorption coefficient $\alpha(\omega)$ as compared to untreated QDs. Generally, it induces strong changes in $\varepsilon_1(\omega)$, $\varepsilon_2(\omega)$, which interestingly leads to the intended positive compromise between diluted oleate-QDs and bulk PbS: For example, the dielectric function at the excitonic energy translates to an absorption coefficient α of QDs with iodide ligands higher than for bulk PbS as indicated in Figure 4c. This effect inverts in the visible and UV range again: Here, QDs treated with iodide approximate the oleate-capped system with both having a comparable lower absorption than bulk PbS. Furthermore, we denote the consistency of the ellipsometric dataset including a Kramers–Kronig relation check

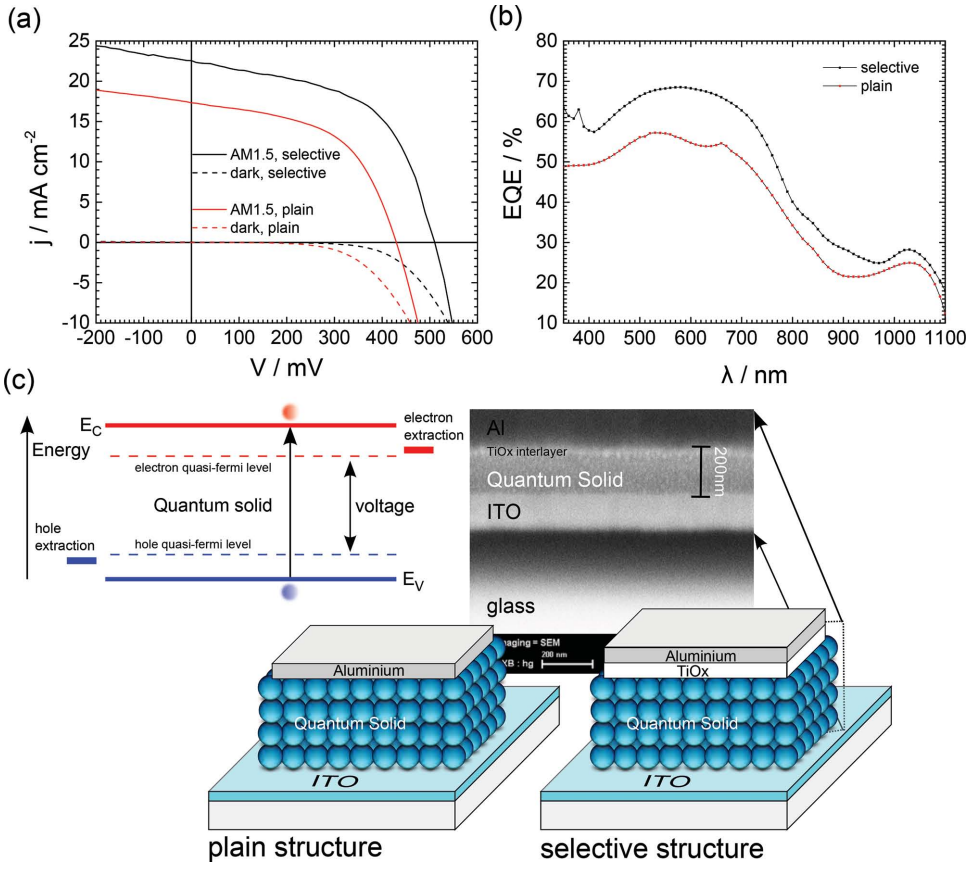

Figure 5. a) The photovoltaic performance of the plain (red) and selective structure solar cell (black) shown in dark and under AM1.5 illumination. b) Spectral EQE is resolved for the plain and selective device structure. c) Photovoltaic device concept and the corresponding cell structures are depicted.

and including fits relying on data from 6 angles of incidence. Hence, QD thin-films—oleate-capped and iodide-treated—describe by a single homogeneous dielectric function in the visible and near-IR spectral region—despite of the fact that the system is inhomogeneous on an atomistic scale.

For employing thin-films in a photovoltaic device, we thought of a straightforward single junction design in order to apply our insight from above. Our concept applies etched ITO (work function 4.7 eV) as hole-selective electrode.[24] We found that QDs processed directly thereon render high-quality thin-films. We modify the film thickness—according to the absorption coefficient the minimum layer thickness is found around 200–250 nm for 90% absorption at the exciton energy. We have characterized different active layer thicknesses and found the highest power conversion efficiency (PCE) at 200 nm. As top contact we have tested plane aluminum first applying the design of Piliego et al.[25] In order to improve on the electron selectivity, we inserted a thin titania contact layer on top—in analogy to commonly used hole-selective molybdenum(IV) oxide. Thin (approximately 8 nm) titania serves as an excellent stable electron-selective contact layer, which can be generated by facile low temperature process. The corresponding *J*–*V* plots and the device design including a cross section SEM are presented in **Figure 5**. The *J*–*V* plots depict the effect of the selective titania contact layer by shifting the open circuit potential to higher values. The external quantum efficiencies in b) reflect the absorption profile of treated QDs from Figure 4c. We used EQE and *J*–*V* to determine photovoltaic device parameters summarized in **Table 1**. The study on varying active layer's thicknesses is shown in the Supporting Information.

The present solar cells exhibit a similar response as reported earlier for record single-layer QD device designs,[26,27] it gives a guideline for a significant and straightforward photovoltaic cell. Further optimization of the interfaces and contacts have yielded only a moderate increase. Our detailed spectroscopic framework in combination with the solar cells rather demonstrated that limitations are inherent in the QD film processing—in particular the ligand treatment. Future projects have to optimize on that part for engineering QD toward improved performances.

In summary, we characterized in detail quantum dot thin-films in terms of their optical properties. Means of

Table 1. Solar cell results measured under illumination.

	PCE [%]	FF [%]	V_{OC} [V]	J_{SC} [mA cm^{-2}]	R_s [Ω]	R_{sh} [kΩ cm^2]
Plain	4.0 ± 0.05	55 ± 1.7	0.43 ± 0.02	17.21 ± 0.07	21 ± 2	11 ± 0.6
Selective	6.0 ± 0.06	53 ± 1.6	0.51 ± 0.02	21.52 ± 0.07	24 ± 3	14 ± 0.57

ellipsometry, time-resolved photoluminescence, and in situ FTIR provide a clear picture on the optical parameters during the entire thin-film process. Using this insights we identify limits in QD thin films. Our spectroscopic view from UV to the mid-IR helps to elaborate the crucial optical parameters during QD processing—furthermore our insights yield precise information of optical parameters and point at the idle potentials to be activated for next-generation QD-based optoelectronic devices.

Quantum dot thin-film solids represent versatile absorbers—with an eye on photovoltaic applications they uniquely combine key-properties such as tunable band edge and strong luminescence as well as facile processing. In this work we outline an in-depth optical description of low-gap semiconductor QDs, that—over a colloidal nanocrystal route—have been size-shifted for optimized absorption, solution-processed, and up-concentrated in a thin-film by ligand-treatment for efficient photon-harvesting. Our multiview step-by-step spectral survey confirm that—finally—QD thin films represent the expected powerful absorber material for solar cells. At the same time we clearly identify the limits of the system, which have to be approached for future optimizations: Namely, quenching say the carrier life time is to-be-improved as well as overtreatment—necking, sintering—that are harmful to the confined states. A more gentle, careful ligand treatment is to our opinion the possible route in order to push quantum dots—with its unique properties—as part to the central material front for powerful photovoltaic cells.

Experimental Section

Thin-Film and Device Fabrication: PbS QDs of 3 nm are fabricated following Hines and Scholes[28] recipe. The final PbS nanocrystals are isolated (acetone wash, redissolving in toluene). The final solution (methanol–ethanol blend (1:1) treatment, redispersion in *n*-hexane, 3 times) has a concentration of 25 mg ml^{-1}. The ligand substitution is performed using a solution of tetrabutylammonium iodide (TBA-I) (Sigma–Aldrich, 0.1 M, 37 mg ml^{-1} in ethanol).

The ITO-slides (1 × 1 in., active area 15 mm^2) are treated with acetone, isopropyl alcohol, Hellmanex (Hellma Inc.) and 0.1 M 1:1 $H_{2>}O_{2>}$:NH_3 (80 °C, 15 min). The absorber layers are prepared as followed: QDs are spin-cast at 900 rpm for 10 s and 4000 rpm for 20 s from 25 mg mL^{-1} hexane solution, then exposed to TBA-I solution twice for 1 min and finally washed with ethanol twice and with toluene once. The process is repeated to the desired thickness accordingly. The single layer is 22 nm thick as measured by a Dektak profilometer (Bruker). The standard active thin-films consist of nine layers (approximately 200 nm). For the titania contact layer the samples are transferred to inert atmosphere first. Then, a precursor layer is deposited by rinsing the active layer with titanium-(IV)-isopropoxide (Sigma–Aldrich) followed by a hexane-wash. The samples are transferred to ambient atmosphere and developed overnight (repeated 3 times). Finally, the devices are annealed (75 °C, 30 min). The top electrode (aluminum, 100 nm) is evaporated under a pressure of 2×10^{-6} mbar.

PV Characterization: The photovoltaic cells are characterized in dark and under simulated AM1.5 solar irradiation using a Steuernagel 575 sun simulator with 100 mW cm^{-2} intensity. A Keithley 236 source meter is used to record the current density–voltage *J–V* characteristics. The spectral photocurrent external quantum efficiency (EQE) is measured using an optical fiber monochromatized xenon-lamp (illumination density 5–10 μW, ACTON Spectra Pro150 monochromator, EG&G 7260 DSP Lock-in amplifier).

Optical Characterization: Transmission measurements are carried out using a Perkin–Elmer T80 UV/VIS spectrophotometer. The photoluminescence (PL) has been characterized using a Photon Technology International optical probing system (excitation wavelength 475 nm). For recording of time-resolved PL spectra the sample is excited with 657 nm laser (pulse width 68 ps at 1 MHz, average power 850 nW). For detection a microscope objective and long-pass bandwidth filter transmitting in near-IR is used (Semiconducting Single Photon Detector (Scontel T = 1.8 K, quantum efficiency 12% at 0.95 eV)). The delay time traces are recorded by Time-Correlated Single Photon Counting PicoHarp 300 (PicoQuant). For the mid-IR study, a ZnSe parallelepiped single crystal (Harrick) serves as substrate for the ATR-FTIR (attenuated total reflection). QDs are deposited directly on top as described above. The ATR-crystal is mounted into the setup (Bruker IFS665S) with an integrated flow-cell. After purging the system with nitrogen a reference spectrum of the as-deposited colloid film is recorded. Then the cell is flushed with TBA-I solution. After 15 min the solution is changed to plain ethanol, flushed another 15 min and finally left 12 h drying in inert atmosphere. Continuously during all steps in situ FTIR-scans are recorded. For the temperature scan the film on top of the ATR-crystal is annealed ex situ in a glovebox at 50, 100, 150, and 200 °C in an oven. After each temperature step the crystal is transferred back to the FTIR-spectrometer and characterized (for details see Supporting Information).

A Wollam M-2000 (with rotating compensator) ellipsometer covering an energy range from 0.73 to 6.5 eV is used to determine the real $\varepsilon_1(\omega)$ and imaginary $\varepsilon_2(\omega)$ part of the dielectric function and absorption coefficient $\alpha(\omega)$ of the active material. The thin layer is prepared on glass and silicon, respectively. The colloid form is tested as-spun - single layer according to the recipe above. In a second run, the same film is characterized after treatment. The ellipsometric measured quantities $\psi(\omega)$ and $\Delta(\omega)$ are recorded at six different angles (variable angle spectroscopic ellipsometry, VASE). The dielectric function is obtained by modeling $\psi(\omega)$ and $\Delta(\omega)$ using Bruggeman of effective medium approximation. In this approach a generic oscillator describing volume PbS and a Cauchy model for oleic acid and iodide are used, respectively.

Supporting Information

Supporting Information is available from the Wiley Online Library or from the author.

Acknowledgements

S.A.M. is grateful to ICTP (International Centre for Theoretical Physics) for financial support in the framework of ANSOLE's (African Network for Solar Energy) ANEX fellowship program. W.H and M.S. acknowledge the Austrian Fund for Advancement of Science (FWF) within project IRON (Infrarered Optical Nanostructures). P.S., S.E., C.E., and N.S.S. gratefully acknowledge the financial support from FWF within the Wittgenstein Prize scheme (Z222-N19 Solare Energieumwandlung).

Received: October 27, 2014
Revised: November 25, 2014
Published online: January 21, 2015

[1] M. G. Panthani, J. M. Kurley, R. W. Crisp, T. C. Dietz, T. Ezzyat, J. M. Luther, D. V. Talapin, *Nano Lett.* **2014**, *14*, 670.
[2] C. J. Stolle, R. D. Schaller, B. A. Korgel, *J. Phys. Chem. C* **2014**, *5*, 3169.
[3] A. H. Ip, S. M. Thon, S. Hoogland, O. Voznyy, D. Zhitomirsky, R. Debnath, L. Levina, L. R. Rollny, G. H. Carey, A. Fischer, K. W. Kemp, I. J. Kramer, Z. Ning, A. J. Labelle, K. W. Chou, A. Amassian, E. H. Sargent, *Nat. Nanotechnol.* **2012**, *7*, 1.

[4] Z. Ning, Y. Ren, S. Hoogland, O. Voznyy, L. Levina, P. Stadler, X. Lan, D. Zhitomirsky, E. H. Sargent, *Adv. Mater.* **2012**, *24*, 6295.
[5] Z. Ning, O. Voznyy, J. Pan, S. Hoogland, V. Adinolfi, J. Xu, M. Li, A. R. Kirmani, J.-P. Sun, J. Minor, K. W. Kemp, H. Dong, L. Rollny, A. Labelle, G. Carey, B. Sutherland, I. Hill, A. Amassian, H. Liu, J. Tang, O. M. Bakr, E. H. Sargent, *Nat. Mater.* **2014**, *13*, 4.
[6] C.-H. M. Chuang, P. R. Brown, V. Bulović, M. G. Bawendi, *Nat. Mater.* **2014**, *13*, 796.
[7] J. Tang, H. Liu, D. Zhitomirsky, S. Hoogland, X. Wang, M. Furukawa, L. Levina, E. H. Sargent, *Nano Lett.* **2012**, *12*, 4889.
[8] A. Nag, M. V. Kovalenko, J.-S. Lee, W. Liu, B. Spokoyny, D. V. Talapin, *J. Am. Chem. Soc.* **2011**, *133*, 10612.
[9] S. M. Thon, A. H. Ip, O. Voznyy, L. Levina, K. W. Kemp, G. H. Carey, S. Masala, E. H. Sargent, *ACS Nano*, **2013**, *7*, 7680.
[10] P. Stadler, B. R. Sutherland, Y. Ren, Z. Ning, A. Simchi, S. M. Thon, S. Hoogland, E. H. Sargent, *ACS Nano* **2013**, *7*, 5757.
[11] D. Zhitomirsky, M. Furukawa, J. Tang, P. Stadler, S. Hoogland, O. Voznyy, H. Liu, E. H. Sargent, *Adv. Mater.* **2012**, *24*, 6181.
[12] V. Rinnerbauer, M. Kovalenko, V. Lavchiev, G. Kocher, J. Roither, W. Heiss, K. Hingerl, *Phys. E (Amsterdam, Neth.)* **2006**, *32*, 104.
[13] V. Rinnerbauer, K. Hingerl, M. Kovalenko, W. Heiss, *Appl. Surf. Sci.* **2007**, *254*, 291.
[14] D. M. Balazs, M. I. Nugraha, S. Z. Bisri, M. Sytnyk, W. Heiss, M. A. Loi, *Appl. Phys. Lett.* **2014**, *104*, 112104.
[15] K. Szendrei, M. Speirs, W. Gomulya, D. Jarzab, M. Manca, O. V. Mikhnenko, M. Yarema, B. J. Kooi, W. Heiss, M. A. Loi, *Adv. Funct. Mater.* **2012**, *22*, 1598.
[16] P. Guyot-Sionnest, *Nat. Mater.* **2005**, *4*, 653.
[17] A. T. Fafarman, S.-H. Hong, H. Caglayan, X. Ye, B. T. Diroll, T. Paik, N. Engheta, C. B. Murray, C. R. Kagan, *Nano Lett.* **2013**, *13*, 350.
[18] T. Yelin, R. Vardimon, N. Kuritz, R. Korytar, A. Bagrets, F. Evers, L. Kronik, O. Tal, *Nano Lett.* **2013**, *13*, 1956.
[19] M. P. Boneschanscher, W. H. Evers, J. J. Geuchies, T. Altantzis, B. Goris, F. T. Rabouw, S. A. P. van Rossum, H. S. J. van der Zant, L. D. a. Siebbeles, G. Van Tendeloo, I. Swart, J. Hilhorst, A. V. Petukhov, S. Bals, D. Vanmaekelbergh, *Science* **2014**, *344*, 1377.
[20] K. S. Jeong, R. D. Pensack, J. B. Asbury, *Acc. Chem. Res.* **2013**, *46*, 1538.
[21] P. Moroz, N. Kholmicheva, B. Mellott, G. Liyanage, U. Rijal, E. Bastola, K. Huband, E. Khon, K. McBride, M. Zamkov, *ACS Nano* **2013**, *7*, 6964.
[22] O. Epshtein, G. Nakhmanovich, Y. Eichen, E. Ehrenfreund, *Phys. Rev. B* **2001**, *63*, 125206.
[23] E. D. Palik, D. L. Mitchell, J. N. Zemel, *Phys. Res.* **1963**, *131*, 763.
[24] N. R. Armstrong, C. Carter, C. Donley, A. Simmonds, P. Lee, M. Brumbach, B. Kippelen, B. Domercq, S. Yoo, *Thin Solid Films* **2003**, *445*, 342.
[25] C. Piliego, L. Protesescu, S. Z. Bisri, M. V. Kovalenko, M. A. Loi, *Energy Environ. Sci.* **2013**, *6*, 3054.
[26] K. Szendrei, W. Gomulya, M. Yarema, W. Heiss, M. A. Loi, *Appl. Phys. Lett.* **2010**, *97*, 203501.
[27] G.-H. Kim, B. Walker, H.-B. Kim, J. Y. Kim, E. H. Sargent, J. Park, *Adv. Mater.* **2014**, *26*, 3321.
[28] M. A. Hines, G. D. Scholes, *Adv. Mater.* **2003**, *15*, 1844.